Turing Patterns in CNNs—Part II: Equations and Behaviors

Liviu Goraş, *Member, IEEE,* and Leon O. Chua, *Fellow, IEEE*

***Abstract*—The general state equations describing two-grid coupled CNNs based on the reduced Chua's circuit are derived, and the analysis of Turing pattern formation is approached from a specific point of view: spatial-eigenfunction based equation decoupling. Discrete spatial eigenfunctions for two common types of boundary conditions are presented, and the way the dynamics is influenced by the shape and position of the dispersion curve is analyzed.**

I. Introduction

In PART I of this paper [1], it was shown that two-grid coupled CNNs based on the reduced Chua's circuit have the potential of producing reaction-diffusion type (Turing) patterns.[1] In the above paper the general principle of pattern formation has been described, the conditions concerning the individual cell have been analyzed, a qualitative explanation of the pattern formation mechanism in a 1-D CNN has been given, and the multiple equilibria property has been exemplified. The key mechanism of pattern formation is based on two kinds of conditions. The first kind refers to requirements for the isolated cells to have a *unique, stable* equilibrium point. These conditions, in terms of the nonlinear characteristic and of the Jacobian matrix of the isolated cell at the equilibrium point, have been derived in [1]. For the whole interconnected array, the above equilibrium is still an equilibrium point but, for pattern formation, it should become unstable; the pattern will correspond to some of the other equilibrium points that happen to be stable. The second kind of conditions, involving not only the cell parameters but also those of the resistive coupling grid will be discussed in this paper after deriving the state equations for the CNN. They are related to a special technique of decoupling the linearized differential equations describing the CNN: spatial-eigenfunction based decoupling. The first step is to derive the state equations of the two-grid coupled CNN subject to the nonstandard normalization introduced in [1].

II. The State Equations of the Two-Grid Coupled CNN

Let us focus on the (i, j) pair of nodes of the array (Fig. 1). Sometimes we will not display explicitly the time dependence.

Manuscript received December 5, 1994; revised March 14, 1995. The work of L. Goraş was supported by the Fulbright Foundation. This paper was recommended by Guest Editor L. O. Chua.

The authors are with the Electronics Research Laboratory, University of California at Berkeley, Berkeley, CA 94720 USA.

IEEE Log Number 9414457.

[1] In the sense of the definition adopted in [1]; i.e., the steady state evolved through a differentiated behavior of identical elements identically coupled in a homogeneous (regular) spatial distribution.

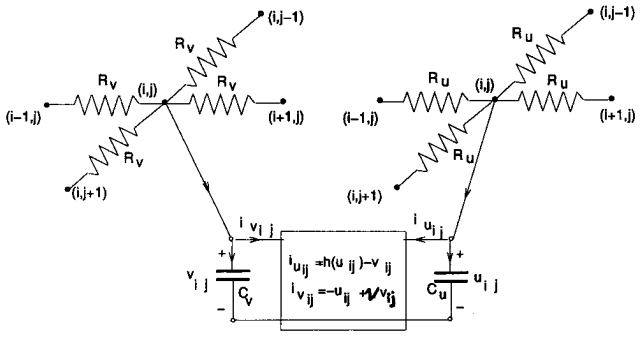

Fig. 1. The (i, j) node of the two-grid coupled CNN.

Notations $u(i, j, t)$, $u_{i,j}(t)$, $u_{i,j}$ will be used interchangeably. Straightforward use of KCL gives

$$\begin{cases} C_u \frac{du_{i,j}(t)}{dt} = -h(u_{ij}) + v_{ij} \\ + G_u[(u_{i+1,j} - u_{i,j}) - (u_{i,j} - u_{i-1,j}) \\ + (u_{i,j+1} - u_{i,j}) - (u_{i,j} - u_{i,j-1})] \\ C_v \frac{dv_{i,j}(t)}{dt} = u_{ij} - \nu v_{ij} \\ + G_v[(v_{i+1,j} - v_{i,j}) - (v_{i,j} - v_{i-1,j}) \\ + (v_{i,j+1} - v_{i,j}) - (v_{i,j} - v_{i,j-1})] \end{cases} \tag{1}$$

where $i = 0, 1, \cdots, M-1, j = 0, 1, \cdots, N-1$. Using the following notations for the 2-D discrete Laplacian[2]

$$\begin{aligned} \nabla^2 u_{i,j} &= [(u_{i+1,j} - u_{i,j}) - (u_{i,j} - u_{i-1,j})] \\ &\quad + [(u_{i,j+1} - u_{i,j}) - (u_{i,j} - u_{i,j-1})] \\ &= u_{i+1,j} + u_{i-1,j} + u_{i,j+1} + u_{i,j-1} - 4u_{i,j} \end{aligned} \tag{2}$$

introducing the "diffusion" coefficients $D_u = \frac{G_u}{C_u}, D_v = \frac{G_v}{C_v}$, and using the notations defined in Part I, the above equations become

$$\boxed{\begin{aligned} \frac{du_{i,j}(t)}{dt} &= \gamma f(u_{i,j}, v_{i,j}) + D_u \nabla^2 u_{i,j} \\ \frac{dv_{i,j}(t)}{dt} &= \gamma g(u_{i,j}, v_{i,j}) + D_v \nabla^2 v_{i,j} \end{aligned}} \tag{3}$$

$i = 0, 1, \cdots, M-1, j = 0, 1, \cdots, N-1$. For certain values of the parameters, the above system of $2MN$ autonomous nonlinear ordinary differential equations describe the simplest two-grid coupled CNNs capable of producing Turing patterns.

[2] In the 1-D case, the discrete 1-D Laplacian is given by $\nabla^2 u_i = (u_{i+1} - u_i) - (u_i - u_{i-1}) = u_{i+1} + u_{i-1} - 2u_i$.

Although (1) are nonlinear, we will show that significant information concerning pattern formation can be obtained from the linearized system in the vicinity of the steady state solution of the isolated cell, which is an equilibrium point for the whole array as well. Linearization of (1) around the equilibrium point (U_0, V_0) gives the following system of *linear* ordinary differential equations:[3]

$$\begin{aligned} \frac{du_{i,j}(t)}{dt} &= \gamma(f_u u_{i,j} + f_v v_{i,j}) + D_u \nabla^2 u_{i,j} \\ \frac{dv_{i,j}(t)}{dt} &= \gamma(g_u u_{i,j} + g_v v_{i,j}) + D_v \nabla^2 v_{i,j} \end{aligned} \tag{4}$$

$i = 0, 1, \cdots, M-1$, $j = 0, 1, \cdots, N-1$, where f_u, f_v, g_u, g_v are the elements of the Jacobian matrix of $f(u, v)$ and $g(u, v)$ corresponding to the equilibrium point (U_0, V_0) chosen on one of the three segments of the piecewise-linear characteristic. Their values as functions of the parameters of the nonlinear resistor in the second-order Chua's circuit are [1]: $f_u = -\frac{|C_u|}{C_u} m_i$ ($i = 0, 1$, or 2 depending on the segment of the piecewise-linear characteristic of Chua's diode the equilibrium point lies in), $f_v = \frac{|C_u|}{C_v}, g_u = \frac{|C_u|}{C_v}, g_v = -\nu\frac{|C_u|}{C_v}$. They must satisfy the relations $f_u + g_v < 0$ and $f_u g_v - f_v g_u > 0$. Equations (4) will be used in the following to analyze the mechanism of Turing pattern formation.

[3]The symbol γ here is unrelated to the one usually associated with Chua's oscillator [2]. This is chosen in order to agree with the usual symbol used in [3].

Standard State Equations Approach: Let us briefly discuss the classical form of the solution of the linear state equations for the two-grid coupled CNNs. The system (4) may be written in various forms depending on the ordering of the variables. As an example, we present at the bottom of this page the equations for the 1-D case ($M = 5$, $N = 1$) where the u's are chosen as the first M variables and the v's as the last M variables.

In the general case, the solution of the linear system of $2MN$ equations, assuming simple eigenvalues, has the well-known form [5]

$$\mathbf{x}(t) = \sum_{i=0}^{2MN-1} \langle \mathbf{r}_i, \mathbf{x}(0) \rangle e^{\lambda_i t} \mathbf{q}_i \tag{6}$$

where $\mathbf{x}(t) = [u_0 u_1 \cdots u_{MN-1} v_0 v_1 \cdots v_{MN-1}]^T$ is the state vector, $\mathbf{q}_i$ are the eigenvectors of the system matrix, $\mathbf{r}_i$ represents the reciprocal basis, $\mathbf{x}(0)$ are the initial conditions, and $\langle ., . \rangle$ denotes the scalar product in $\mathbf{C}^n$ ($n = 2MN$). We recognize the well-known behavior of the solution: a weighted sum of exponentials (having the exponents determined by the $2MN$th-order characteristic equation of the system), the weighting coefficient being dependent on the initial conditions. This solution, which can be written for any linear system of differential equations having distinct eigenvalues, shows the possibility of having unstable modes if some λ_i have positive real parts. We could make a change of variables to decouple the equations by diagonalizing the matrix of the system or reducing it to a canonical Jordan form. In this way,

$$\begin{bmatrix} \dot{u}_0 \\ \dot{u}_1 \\ \dot{u}_2 \\ \dot{u}_3 \\ \dot{u}_4 \\ \dot{v}_0 \\ \dot{v}_1 \\ \dot{v}_2 \\ \dot{v}_3 \\ \dot{v}_4 \end{bmatrix} = \begin{bmatrix} \gamma f_u - D_u & D_u & 0 & 0 & 0 & \gamma f_v & 0 & 0 & 0 & 0 \\ D_u & \gamma f_u - 2D_u & D_u & 0 & 0 & 0 & \gamma f_v & 0 & 0 & 0 \\ 0 & D_u & \gamma f_u - 2D_u & D_u & 0 & 0 & 0 & \gamma f_v & 0 & 0 \\ 0 & 0 & D_u & \gamma f_u - 2D_u & D_u & 0 & 0 & 0 & \gamma f_v & 0 \\ 0 & 0 & 0 & D_u & \gamma f_u - D_u & 0 & 0 & 0 & 0 & \gamma f_v \\ \gamma g_u & 0 & 0 & 0 & 0 & \gamma g_v - D_v & D_v & 0 & 0 & 0 \\ 0 & \gamma g_u & 0 & 0 & 0 & D_v & \gamma g_v - 2D_v & D_v & 0 & 0 \\ 0 & 0 & \gamma g_u & 0 & 0 & 0 & D_v & \gamma g_v - 2D_v & D_v & 0 \\ 0 & 0 & 0 & \gamma g_u & 0 & 0 & 0 & D_v & \gamma g_v - 2D_v & D_v \\ 0 & 0 & 0 & 0 & \gamma g_u & 0 & 0 & 0 & D_v & \gamma g_v - D_v \end{bmatrix} \times \begin{bmatrix} u_0 \\ u_1 \\ u_2 \\ u_3 \\ u_4 \\ v_0 \\ v_1 \\ v_2 \\ v_3 \\ v_4 \end{bmatrix} \tag{5}$$

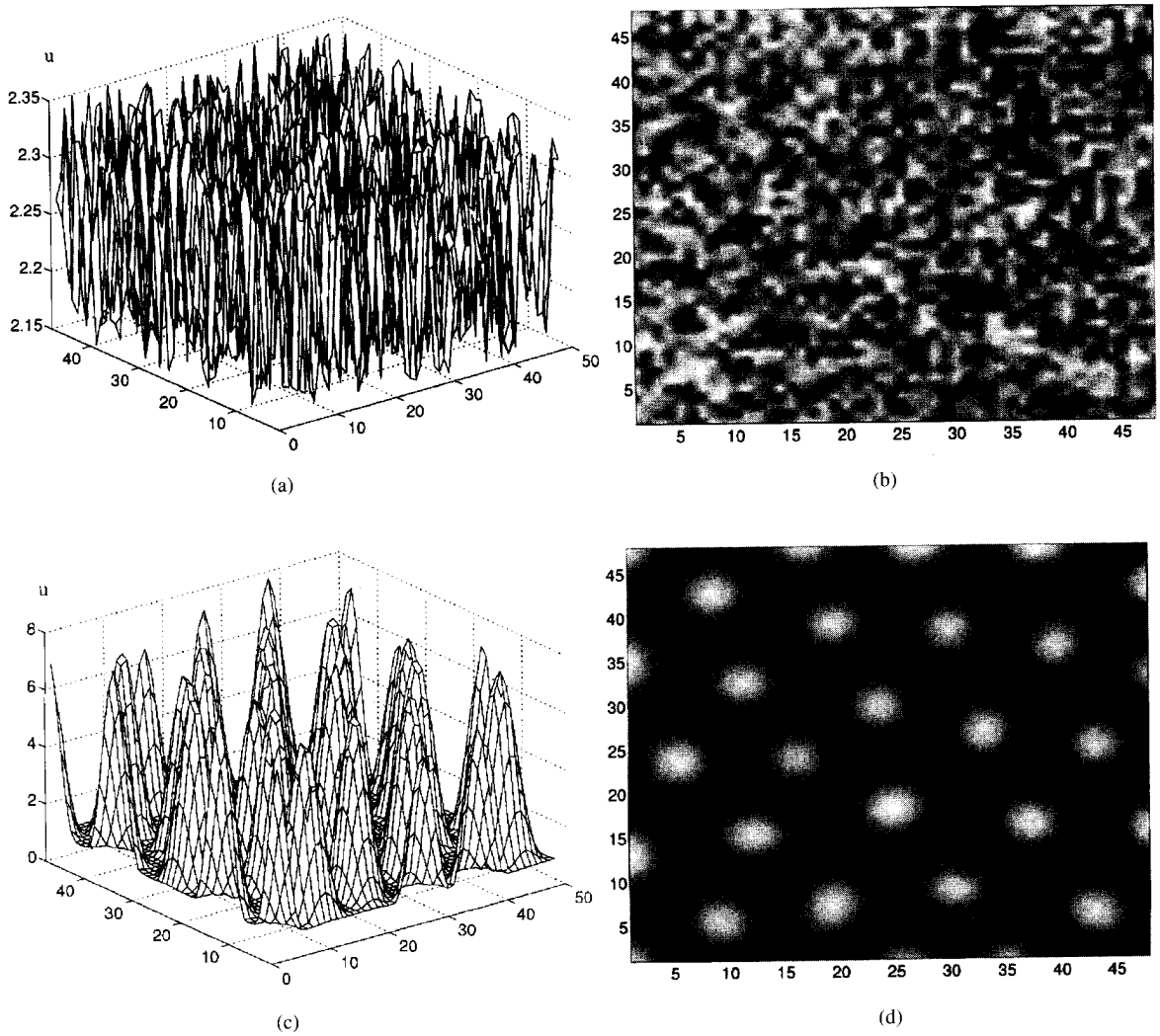

Fig. 2. (a) Three-dimensional and (b) two dimensional representations of the incipient phase of pattern formation in a 50 × 50 array of two-grid coupled CNN made of second-order Chua's circuits under random initial conditions. (c) and (d) Final Turing patterns.

we could separate the stable modes from the unstable modes, but the new state variables would be linear combinations of the node voltages of the cells, and no relations to patterns could be made. However, in this case, we would have to face the problem of handling a very high-order characteristic polynomial, which is completely impractical. In the next section of this paper, we will use another way of separating the stable from the unstable modes with direct relation to pattern formation.

In general, the linear theory can predict only how the pattern begins to evolve. From this point of view, the piecewise-linear character of the nonlinearity is very convenient. However, when the amplitude grows, the nonlinearities enter the scene, and the linear predictions are no longer valid. To illustrate the evolution of a pattern, we present, in Fig. 2(a) and (b), the initial stage of pattern formation and, in Fig. 2(c) and (d), the final Turing pattern for a two-grid coupled CNN consisting of a 50 × 50 array of second-order Chua's circuits ($\gamma = 10, m_0 = -1, m_1 = 0.1, \nu = 2, C_u = -0.1, C_v = 1, \epsilon = 2$), subject to random initial conditions for both u and v variables. In all figures, only the u variable is displayed, and interpolation has been used for the display.

III. Decoupling of Linearized State Equations

The essence of the technique in this section is to transform the original system of $2MN$-*coupled* differential equations to MN-*uncoupled* systems of two first-order linear differential equations, no matter how big M and N are. Moreover, the new variables have a direct relation to the emerging pattern.

A. The 1-D Case

We first present in detail the solution to a 1-D CNN composed of M cells. The 2-D case follows by direct generalization. The main idea of this technique is to look for a solution of the system (4) as a weighted sum of M space-dependent functions[4] $\phi_M(m,i)$, the eigenfunctions of the *discrete* Laplacian,

$$\nabla^2\phi_M(m,i) = \phi_M(m,i+1) + \phi_M(m,i-1) - 2\phi_M(m,i) = -k_m^2\phi_M(m,i) \quad (7)$$

where k_m^2 are the corresponding eigenvalues. The exponent 2 associated with k_m is usually introduced in the literature

[4]The first argument m should be regarded as a summation index, and the second one as the current space variable.

because the eigenvalues are proportional to the square (or the sum of squares) of sine functions. The negative sign associated with k_m in (7) is usually introduced so that k_m^2 is a positive number at least for the zero-flux and periodic boundary conditions (see Appendix II). Thus, we look for the general solution of the system (4) in the form

$$\begin{cases} u_i(t) = \sum_{m=0}^{M-1} \phi_M(m,i)\hat{u}_m(t) \\ v_i(t) = \sum_{m=0}^{M-1} \phi_M(m,i)\hat{v}_m(t) \end{cases} \quad i = 0,1,\cdots,M-1. \tag{8}$$

The temporal and spatial variables in (8) are separated in the sense that the weighting coefficients $\hat{u}_m$ and $\hat{v}_m$ are (only) time dependent (even though we will not always explicitly show the time dependence) while the spatial eigenfunctions $\phi_M(m,i)$ are only space dependent. A supplementary property required for $\phi_M(m,i)$ is that they should satisfy the boundary conditions for all m, so that any linear combination of such functions will also satisfy the boundary conditions. To simplify our derivations, it is desirable to choose the eigenfunctions to be orthonormal; namely,

$$\langle \phi_M(m,i), \phi_M(n,i) \rangle = \delta_{mn} \tag{9}$$

where δ_{mn} denotes the Kronecker symbol and

$$\langle a,b \rangle = \sum_{i=0}^{M-1} a_i^* b_i \tag{10}$$

denotes the scalar product in $\mathbf{C}^M$, where the asterisk denotes complex conjugation. We need the complex form of the scalar product because the eigenfunctions are generally complex as in the case of a *periodic* (ring) boundary condition. The final solutions will be real due to cancellations of imaginary parts.

Taking the scalar product of each of (8) with $\phi_M(n,i)$ we find that, due to (9)

$$\begin{cases} \hat{u}_n = \sum_{i=0}^{M-1} \phi_M^*(n,i) u_i \\ \hat{v}_n = \sum_{i=0}^{M-1} \phi_M^*(n,i) v_i \end{cases} \tag{11}$$

$n = 0,1,\cdots,M-1$. Readers familiar with linear vector space or signal theory will recognize that $\hat{u}_n$ and $\hat{v}_n$ are the spectrum of u_i and v_i with respect to the orthonormal basis $\{\phi_M(n,i); (n = 0,1,\cdots,M-1,\ i = 0,1,\cdots,M-1)\}$. Imposing the condition that the functions given by (8) satisfy the system of (linear) differential equations that describe the CNN, we have

$$\begin{bmatrix} \sum_{m=0}^{M-1} \phi_M(m,i)\dot{\hat{u}}_m \\ \sum_{m=0}^{M-1} \phi_M(m,i)\dot{\hat{v}}_m \end{bmatrix} = \gamma \begin{bmatrix} f_u & f_v \\ g_u & g_v \end{bmatrix} \begin{bmatrix} \sum_{m=0}^{M-1} \phi_M(m,i)\hat{u}_m \\ \sum_{m=0}^{M-1} \phi_M(m,i)\hat{v}_m \end{bmatrix} + \begin{bmatrix} D_u & 0 \\ 0 & D_v \end{bmatrix} \begin{bmatrix} \sum_{m=0}^{M-1} -k_m^2 \phi_M(m,i)\hat{u}_m \\ \sum_{m=0}^{M-1} -k_m^2 \phi_M(m,i)\hat{v}_m \end{bmatrix}. \tag{12}$$

Taking successively the scalar product of both sides of (12) with $\phi_M^*(n,i)$ and using again m as the current index, we obtain the following M pairs of linear differential equations

$$\begin{bmatrix} \dot{\hat{u}}_m \\ \dot{\hat{v}}_m \end{bmatrix} = \gamma \begin{bmatrix} f_u & f_v \\ g_u & g_v \end{bmatrix} \begin{bmatrix} \hat{u}_m \\ \hat{v}_m \end{bmatrix} - k_m^2 \begin{bmatrix} D_u & 0 \\ 0 & D_v \end{bmatrix} \begin{bmatrix} \hat{u}_m \\ \hat{v}_m \end{bmatrix} \tag{13}$$

$m = 0,1,\cdots,M-1$. The solutions of (13) have the form

$$\begin{cases} \hat{u}_m = a_m e^{\lambda_{m_1} t} + b_m e^{\lambda_{m_2} t} \\ \hat{v}_m = c_m e^{\lambda_{m_1} t} + d_m e^{\lambda_{m_2} t} \end{cases} \tag{14}$$

where λ_{m_1} and λ_{m_2} are the roots of the characteristic equations

$$\det\left\{ \lambda_m \begin{bmatrix} 1 & 0 \\ 0 & 1 \end{bmatrix} - \gamma \begin{bmatrix} f_u & f_v \\ g_u & g_v \end{bmatrix} + k_m^2 \begin{bmatrix} D_u & 0 \\ 0 & D_v \end{bmatrix} \right\} = 0 \tag{15}$$

i.e.,

$$\lambda_m^2 + \lambda_m[k_m^2(D_u + D_v) - \gamma(f_u + g_v)] + D_u D_v k_m^4 - \gamma(D_v f_u + D_u g_v)k_m^2 + \gamma^2(f_u g_v - f_v g_u) = 0 \quad m = 0,1,\cdots,M-1 \tag{16}$$

and a_m, b_m, c_m, d_m are constants depending on the initial conditions. Thus, using (14), we can write the solution of the 1-D linearized CNN equations (4) in the following form with *separated* spatial variables

$$\begin{aligned} u_i(t) &= \sum_{m=0}^{M-1} (a_m e^{\lambda_{m_1} t} + b_m e^{\lambda_{m_2} t}) \phi_M(m,i) \\ v_i(t) &= \sum_{m=0}^{M-1} (c_m e^{\lambda_{m_1} t} + d_m e^{\lambda_{m_2} t}) \phi_M(m,i). \end{aligned} \tag{17}$$

Observe that the roots of the characteristic equation (16) depend on the spatial eigenvalues k_m^2; for each spatial eigenvalue, there are two roots of the corresponding characteristic equation.

B. The 2-D Case

The 2-D problem can be approached in a similar manner: find MN orthonormal functions $\phi_{MN}(m,n,i,j)$ and the same number of eigenvalues k_{mn}^2 satisfying the relations

$$\begin{aligned} &\nabla^2 \phi_{MN}(m,n,i,j) \\ &\quad = \phi_{MN}(m,n,i+1,j) + \phi_{MN}(m,n,i-1,j) \\ &\qquad + \phi_{MN}(m,n,i,j+1) + \phi_{MN}(m,n,i,j-1) \\ &\qquad - 4\phi_{MN}(m,n,i,j) \\ &\quad = -k_{mn}^2 \phi_{MN}(m,n,i,j) \end{aligned} \tag{18}$$

$$\langle \phi_{MN}(m,n,i,j), \phi_{MN}(p,q,i,j) \rangle = \delta_{mnpq} \tag{19}$$

$$\langle a,b \rangle = \sum_{i=0}^{M-1} \sum_{j=0}^{N-1} a_{ij}^* b_{ij}. \tag{20}$$

Using the relations

$$\begin{cases} u_{i,j} = \sum_{m=0}^{M-1} \sum_{n=0}^{N-1} \phi_{MN}(m,n,i,j)\hat{u}_{m,n} \\ v_{i,j} = \sum_{m=0}^{M-1} \sum_{n=0}^{N-1} \phi_{MN}(m,n,i,j)\hat{v}_{m,n} \end{cases} \quad i = 0,1,\cdots,M-1; j = 0,1,\cdots,N-1 \tag{21}$$

$$\begin{cases} \hat{u}_{m,n} = \sum_{i=0}^{M-1}\sum_{j=0}^{N-1} \phi^*_{MN}(m,n,i,j)u_{i,j} \\ \hat{v}_{m,n} = \sum_{i=0}^{M-1}\sum_{j=0}^{N-1} \phi^*_{MN}(m,n,i,j)v_{i,j} \end{cases}$$
$$m = 0,1,\cdots,M-1; n = 0,1,\cdots,N-1 \quad (22)$$

and following the same procedure as above we find that our problem reduces to solving the following MN pairs of linear differential equations

$$\begin{bmatrix} \dot{\hat{u}}_{m,n} \\ \dot{\hat{v}}_{m,n} \end{bmatrix} = \gamma \begin{bmatrix} f_u & f_v \\ g_u & g_v \end{bmatrix} \begin{bmatrix} \hat{u}_{m,n} \\ \hat{v}_{m,n} \end{bmatrix} - k^2_{mn} \begin{bmatrix} D_u & 0 \\ 0 & D_v \end{bmatrix} \begin{bmatrix} \hat{u}_{m,n} \\ \hat{v}_{m,n} \end{bmatrix} \quad (23)$$

$m = 0,1,\cdots,M-1; n = 0,1,\cdots,N-1$. The solutions have the form

$$\begin{cases} \hat{u}_{m,n} = a_{mn}e^{\lambda_{mn_1}t} + b_{mn}e^{\lambda_{mn_2}t} \\ \hat{v}_{m,n} = c_{mn}e^{\lambda_{mn_1}t} + d_{mn}e^{\lambda_{mn_2}t} \end{cases} \quad (24)$$

where λ_{mn_1} and λ_{mn_2} are the solutions of the characteristic equations

$$\det\left\{ \lambda_{mn} \begin{bmatrix} 1 & 0 \\ 0 & 1 \end{bmatrix} - \gamma \begin{bmatrix} f_u & f_v \\ g_u & g_v \end{bmatrix} + k^2_{mn} \begin{bmatrix} D_u & 0 \\ 0 & D_v \end{bmatrix} \right\} = 0 \quad (25)$$

i.e.,

$$\lambda^2_{mn} + \lambda_{mn}[k^2_{mn}(D_u + D_v) - \gamma(f_u + g_v)] + D_uD_vk^4_{mn} - \gamma(D_vf_u + D_ug_v)k^2_{mn} + \gamma^2(f_ug_v - f_vg_u) = 0,$$
$$m = 0,1,\cdots,M-1; n = 0,1,\cdots,N-1 \quad (26)$$

where $a_{mn}, b_{mn}, c_{mn}, d_{mn}$ are constants depending on the initial conditions.

Consequently, the solution of the linearized 2-D CNN equations (4) has the form as (17). (See (27) at the bottom of this page.)

Equations (17) and (27) are important because the node voltages are expressed in terms of the spatial eigenfunctions; *there is a relation between the spatial eigenfunctions and the temporal eigenvalues of the network.* The equations give the node voltages of the CNN as time-dependent weighted sums of spatial eigenfunctions. To have patterns, it is necessary that at least one of the temporal eigenvalues have a positive real part. For instance, if it is known that a particular temporal eigenvalue has a positive real part, then it follows that the spatially homogeneous equilibrium point is unstable and the corresponding spatial eigenfunction will increase with time until bounded by the nonlinearity. In this case, the dynamics will tend to a pattern *assuming* the CNN has *another* equilibrium point that is stable.

C. Discrete Spatial Eigenvectors

In this section, we consider the spatial eigenvector problem and specify the form of the eigenfunctions $\phi_M(m,i)$ and $\phi_{MN}(m,n,i,j)$ that have already been used without details. Let us first recall the conditions that the functions $\phi_M(m,n)$ have to satisfy; they must be the M eigenvectors of the discrete Laplacian for given boundary conditions and orthonormal with respect to the $\mathbf{C}^M$ scalar product. In the following, we shall present two sets of discrete eigenfunctions that satisfy the above requirements, for two typical types of boundary conditions; namely, *zero-flux* and *periodic* (ring) boundary conditions.[5] We show in Appendix II that the discrete exponential functions are eigenfunctions of the discrete Laplacian operator and, as a consequence, any discrete sine or cosine function is an eigenfunction as well. However, we shall choose those eigenfunctions that satisfy the prescribed boundary conditions.

Discrete 1-D Spatial Eigenfunctions for Zero-Flux Boundary Conditions: In this case, the eigenfunction are the M kernel functions of the Discrete Cosine Transform [6] which is defined by the relations

$$\begin{cases} u_i = \frac{2}{M}\sum_{m=0}^{M-1} e[i]\hat{u}_m \cos\frac{(2i+1)m\pi}{2M} \\ \hat{u}_m = \sum_{i=0}^{M-1} e[i]u_i \cos\frac{(2i+1)m\pi}{2M} \end{cases} \quad (28)$$

where $e[0] = \frac{1}{\sqrt{2}}; e[i] = 1$ for $i \neq 0$. One easily checks that

$$\nabla^2_1 \cos\frac{(2i+1)m\pi}{2M} = -4\sin^2\frac{m\pi}{2M}\cos\frac{(2i+1)m\pi}{2M} \quad (29)$$

i.e., the eigenfunctions and eigenvalues are, respectively,

$$\phi_M(m,i) = \cos\frac{(2i+1)m\pi}{2M}; \quad k^2_m = 4\sin^2\frac{m\pi}{2M}. \quad (30)$$

The eigenfunctions satisfy the zero-flux boundary conditions

$$\phi_M(m,-1) = \phi_M(m,0)$$
$$\phi_M(m,M-1) = \phi_M(m,M) \quad (31)$$

and are orthogonal in the interval $[0, M-1]$.

Remark: We warn the reader that k^2_m as well as k^2_{mn} (in the 2-D case) have, in this paper, the significance of *eigenvalues* of the corresponding discrete Laplacian and *not* wave numbers—a term used in some papers, including [4]. This remark applies to all discrete spatial eigenfunctions that are discussed below too.

[5]The families of functions we are going to present are in fact only orthogonal, not orthonormal; this fact, however, does not affect the preceding derivations.

$$u_{i,j} = \sum_{m=0}^{M-1}\sum_{n=0}^{N-1}(a_{mn}e^{\lambda_{mn_1}t} + b_{mn}e^{\lambda_{mn_2}t})\phi_{MN}(m,n,i,j)$$
$$v_{i,j} = \sum_{m=0}^{M-1}\sum_{n=0}^{N-1}(c_{mn}e^{\lambda_{mn_1}t} + d_{mn}e^{\lambda_{mn_2}t})\phi_{MN}(m,n,i,j). \quad (27)$$

Discrete 1-D Spatial Eigenfunctions for Periodic Boundary Conditions: In this case, the eigenfunctions are the discrete sines and cosines, or the complex exponential kernel functions of the Discrete Fourier Transform [7] defined via

$$\begin{cases} u_i = \frac{1}{M}\sum_{m=0}^{M-1} \hat{u}_m e^{j\frac{2\pi}{M}mi} \\ \hat{u}_m = \sum_{i=0}^{M-1} u_i e^{-j\frac{2\pi}{M}mi}. \end{cases} \tag{32}$$

The eigenfunctions and the eigenvalues are, respectively,

$$\phi_M(m,i) = e^{j\frac{2\pi}{M}mi} \tag{33}$$

$$k_m^2 = 4\sin^2\frac{\pi m}{M}. \tag{34}$$

We remark that the number of distinct eigenvalues in (34) is smaller than in the previous cases because of the smaller period of the sine. However, the number of real eigenvectors is M; to each distinct eigenvalue correspond a sine and a cosine.

Discrete Spatial Eigenfunctions for the 2-D Case: The above results can be easily extended to the 2-D case using the following simple rules:

$$\phi_{MN}(m,n,i,j) = \phi_M(m,i)\phi_N(n,j) \tag{35}$$

$$k_{mn}^2 = k_m^2 + k_n^2 \tag{36}$$

or, in words, *multiply* the eigenvectors and *add* the eigenvalues. Indeed,

$$\begin{aligned} &\nabla^2\phi_M(m,i)\phi_N(n,j) \\ &= [\phi_M(m,i+1) + \phi_M(m,i-1) - 2\phi_M(m,i)]\phi_N(n,j) \\ &\quad + \phi_M(m,i)[\phi_N(n,j+1) + \phi_N(n,j-1) - 2\phi_N(n,j)] \\ &= \nabla_1^2\phi_M(m,i)\cdot\phi_N(n,j) + \phi_M(m,i)\nabla_1^2\phi_N(n,j) \\ &= -k_m^2\phi_M(m,i)\phi_N(n,j) - k_n^2\phi_M(m,i)\phi_N(n,j) \\ &= -(k_m^2 + k_n^2)\phi_M(m,i)\phi_N(n,j) \\ &= -k_{mn}^2\phi_{mn}(m,n,i,j). \end{aligned}$$

For example, the zero-flux spatial eigenvectors and eigenvalues are defined by the relation

$$\begin{aligned} &\nabla^2\cos\frac{(2i+1)m\pi}{2M}\cos\frac{(2j+1)n\pi}{2N} \\ &= -4\Big(\sin^2\frac{m\pi}{2M} + \sin^2\frac{n\pi}{2N}\Big) \\ &\quad\times\cos\frac{(2i+1)m\pi}{2M}\cos\frac{(2j+1)n\pi}{2N}. \end{aligned}$$

From this relation, we identify

$$\begin{aligned} \phi_{MN}(m,n,i,j) &= \cos\frac{(2i+1)m\pi}{2M}\cos\frac{(2j+1)n\pi}{2N} \\ k_{mn}^2 &= 4\Big(\sin^2\frac{m\pi}{2M} + \sin^2\frac{n\pi}{2N}\Big). \end{aligned} \tag{37}$$

The 2-D equivalent of the ring is the torus; the spatial eigenvectors and the corresponding eigenvalues are defined by the relation

$$\nabla^2 e^{j\frac{2\pi}{M}mi}e^{j\frac{2\pi}{N}ni} = -4\Big(\sin^2\frac{m\pi}{M} + \sin^2\frac{n\pi}{N}\Big)e^{j\frac{2\pi}{M}mi}e^{j\frac{2\pi}{N}ni}.$$

From this relation, we identify

$$\begin{aligned} \phi_{MN}(m,n,i,j) &= e^{j\frac{2\pi}{M}mi}e^{j\frac{2\pi}{N}ni} \\ k_{mn}^2 &= 4\Big(\sin^2\frac{m\pi}{M} + \sin^2\frac{n\pi}{N}\Big). \end{aligned} \tag{38}$$

Of course, in the 2-D case, the number of eigenvalues will be much greater than in the 1-D case, making the problem of explaining and predicting the patterns more difficult.

D. Initial Conditions

In the following, we refer to the 2-D case for which there are $4MN$ constants[6] a_{mn}, b_{mn}, c_{mn}, d_{mn}, $m = 0,1,\cdots,M-1$, $n = 0,1,\cdots,N-1$ corresponding to the $2MN$ independent initial conditions $u_0,\cdots,u_{MN-1}, v_0,\cdots,v_{MN-1}$ (voltages of the $2MN$ capacitors of the array). Using (23) and (24) for $t = 0$, we obtain (39) (shown at the bottom of this page) where λ_{mn_1} and λ_{mn_2} must satisfy the characteristic equation (written in a slightly modified form)

$$\begin{cases} (\lambda_{mn_1} - \gamma f_u + D_u k^2)(\lambda_{mn_1} - \gamma g_v + D_v k^2) = \gamma f_v g_u \\ (\lambda_{mn_2} - \gamma f_u + D_u k^2)(\lambda_{mn_2} - \gamma g_v + D_v k^2) = \gamma f_v g_u \end{cases}. \tag{40}$$

It follows from (40) that the constants $a_{mn}, b_{mn}, c_{mn}, d_{mn}$ must satisfy the relations

$$\begin{cases} a_{mn}(\lambda_{mn_1} - \gamma f_u + D_u k_{mn}^2) = c_{mn}\gamma f_v \\ b_{mn}(\lambda_{mn_2} - \gamma f_u + D_u k_{mn}^2) = d_{mn}\gamma f_v \end{cases} \tag{41}$$

or

$$\begin{aligned} &(\lambda_{mn_1} - \gamma f_u + D_u k_{mn}^2)a_{mn}d_{mn} \\ &\quad = (\lambda_{mn_2} - \gamma f_u + D_u k_{mn}^2)b_{mn}c_{mn}. \end{aligned} \tag{42}$$

Using the above relations and taking $t = 0$ in (27) so that $u_{ij} = u_{ij}(0)$ and $v_{ij} = v_{ij}(0)$, all constants can be determined uniquely. In the case of double roots $\lambda_{mn_1} = \lambda_{mn_2} = \lambda_{mn}$,

[6] Obviously not independent.

$$\begin{cases} a_{mn}\lambda_{mn_1} + b_{mn}\lambda_{mn_2} = (a_{mn} + b_{mn})(\gamma f_u - D_u k_{mn}^2) + \gamma f_v(c_{mn} + d_{mn}) \\ c_{mn}\lambda_{mn_1} + d_{mn}\lambda_{mn_2} = (c_{mn} + d_{mn})(\gamma g_v - D_v k_{mn}^2) + \gamma g_u(a_{mn} + b_{mn}) \end{cases} \tag{39}$$

(41) and (42) remain valid upon replacing factors of the form $a_{mn}e^{\lambda_{mn_1}t} + b_{mn}e^{\lambda_{mn_2}t}$ and terms similar to the above by $(a_{mn} + b_{mn}t)e^{\lambda_{mn}t}$.

IV. Pattern Formation

We will now use (16) and (26) to explain the mechanism of pattern formation. These equations give the relation between the spatial and temporal eigenvalues and thus using (17) and (27), we can plot an image of the dynamics via the amplitudes of the spatial modes that are basically cosines and sines. We refer in the following to the 2-D case; all equations and results for the 1-D case are of the same form except for the fact that 1-D eigenvectors should be used.[7]

The scenario of pattern formation is as follows. Due to nonzero initial conditions, the CNN node voltages will vary in time according to (27) in the 2-D case; i.e., each node voltage will be a weighted sum of $2MN$ modes, each pair of modes influencing the amplitude of a certain spatial eigenfunction. Thus, the coefficients $a_{mn}, b_{mn}, c_{mn}, d_{mn}$ (which have been shown to be related and dependent on the initial conditions) will determine the weights of the spatial eigenvectors and the temporal eigenvalues $\lambda_{mn_1}, \lambda_{mn_2}$ will determine the type of initial dynamics: increasing exponentials for positive real-part modes and decreasing exponentials for negative real-part modes. Should any of the above coefficients be zero, the corresponding mode will not appear in the node voltages.[8] Turing patterns can develop when at least one temporal mode has a positive real part. When more than one temporal eigenvalue is in the right-half plane (which is common for large arrays) a competition between modes will appear. Of course, the process will become nonlinear, and the final pattern will be decided by the nonlinearity. Eventually, it may resemble some (distorted) spatial eigenvector or (distorted) combinations of such eigenvectors. The nonlinearity may produce "intermodulation" terms (new eigenvectors resulting from the nonlinear interaction of the initial ones) that influence the final pattern. In this competition of spatial modes (in which, due to the nonlinearity new terms can be born), beside the nonlinearity, two factors are significant too: the initial values of the corresponding temporal modes and the values of the real parts of the temporal eigenvalues. The intuitive feeling that the spatial mode corresponding to the most positive real part of the temporal eigenvalue will eventually win does not always happen in practice; the weights of the increasing exponential terms are also important, and they depend on the initial conditions. The advantage of using the piecewise-linear nonlinearity is that predictions based on linear theory are likely to be valid for a large range of voltages and remain valid sometimes (mainly for small-dimensional arrays and especially in the 1-D case) even after the nonlinearity has played its role. The technique of separating the variables can be used to analyze the nonlinear behavior too, but in this case, the differential equations defining the dynamics of the amplitude of the spatial modes are now nonlinear and no longer decoupled.

[7] Similar formulas can be derived for the continuous space cases too.

[8] This is a linear theory result and is valid until the first cell voltage enters in a nonlinear region. Due to the nonlinear interactions of the spatial modes, the final pattern may contain spatial components that did not previously exist in the initial conditions.

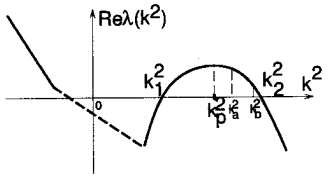

Fig. 3. Typical dispersion curve.

A. The Dispersion Curve

From the above discussion, it should be clear that patterns are determined by the temporal eigenvalues with a positive real part. The graph of the dependence on k^2_{mn} of the temporal eigenvalues having the most positive real part is called the *dispersion curve* [3] and is described by the relation (43), shown at the bottom of the page.

We chose the positive sign of the square root as we are interested in the eigenvalue having the greatest positive real part. The contribution of the eigenvalues having negative real parts will tend to zero as time increases. The index mn was parenthesized because the dispersion curve will be traced as a *continuous* function of k^2 and then samples will be taken at admissible k^2_{mn}. In the subsequent relations, the index mn will be dropped, but we should remember that only MN (M, in the 1-D case) values of $k^2 = k^2_{mn}$ are possible; i.e., only samples of $\mathrm{Re}\lambda(k^2)$ for $k^2 = k^2_{mn}$ are relevant. Thus, the relation (43) (shown at the bottom of this page) gives, for *each* k^2_{mn}, the value of the most positive real part of the eigenvalues associated with k^2_{mn}. Observe that the dispersion curve is uniquely defined by 7 parameters only: f_u, g_u, f_v, g_v, γ, D_u, and D_v. The *spatial* eigenvalues k^2_{mn} depend only on m, n, M, N, and the boundary conditions and do *not* depend on any of the parameters of the dispersion curve. Table II containing the spatial eigenvalues k^2_{mn} for the case $M = 5$ and $N = 6$ is presented in Appendix I.

A typical dispersion curve is shown in Fig. 3. The dashed line represents the locus of $\gamma\left(\frac{f_u+g_v}{2}\right) - k^2_{(mn)}\left(\frac{D_u+D_v}{2}\right)$; namely, the real part of the eigenvalue (which is *complex* within the dashed interval). The interval between k_1^2 and k_2^2 represents the *band of unstable modes* corresponding to real positive roots of the characteristic equation.[9]

[9] Those that happen to lie in that interval, if any.

$$\mathrm{Re}\lambda(k^2_{(mn)}) = \mathrm{Re}\left\{\gamma\frac{(f_u+g_v)}{2} - k^2_{(mn)}\frac{(D_u+D_v)}{2} + \sqrt{\left[\gamma\left(\frac{g_v-f_u}{2}\right) + k^2_{(mn)}\frac{(D_u-D_v)}{2}\right]^2 + \gamma^2 f_v g_u}\right\}. \quad (43)$$

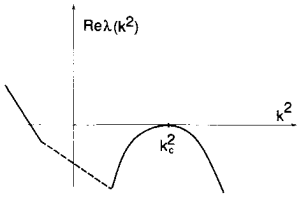

Fig. 4. Critical value of k.

Observe that, for $m = n = 0$, (36)–(38) give $k_{00}^2 = 0$ so that the conditions $f_u + g_v < 0$ and $f_u g_v - f_v g_u > 0$ already imposed for the stability of the isolated cell also ensure that the constant spatial mode will be stable; i.e., $\mathrm{Re}\lambda(0) < 0$ in view of (26) with $k_{mn}^2 = 0$. This is why the dashed line of the dispersion curve must intersect the vertical axis at some point below the origin. There is no contradiction between the fact that the zero spatial mode is stable and the statement made in [1] that the equilibrium point of the CNN corresponding to (U_0, V_0) for all coupled cells must be unstable. In fact, the instability of that equilibrium point ensures the pattern development while the fact that the zero spatial mode is stable ensures that the spatially homogeneous pattern will damp out in time, giving rise to a nontrivial Turing pattern.

Thus, to have patterns, besides the previous two conditions, we should impose that there exist values $k_{mn}^2 \neq 0$ for which $\mathrm{Re}\lambda(k_{mn}^2) > 0$; i.e., *there exists an interval (band) of unstable modes*. This happens if the following two conditions are fulfilled:

$$\begin{cases} D_v f_u + D_u g_v > 0 \\ (D_v f_u - D_u g_v)^2 + 4 D_u D_v f_v g_u > 0. \end{cases} \tag{44}$$

Conditions (44) can be derived by analyzing (26). Such an equation has positive real part roots if one or two of its coefficients are negative. As from previous conditions, the coefficient of λ_{mn} is positive for all k_{mn}^2, the only possibility is to impose k_{mn}^2 such that the constant term is negative. A necessary condition is $D_v f_u + D_u g_v > 0$. Another condition is that the minimum of the above constant term with respect to k_{mn}^2 be negative; i.e., the second condition in (44).

Summarizing, the *necessary* conditions for Turing pattern formation in two-grid coupled CNNs are

$$\begin{aligned} &f_u + g_v < 0 \\ &f_u g_v - f_v g_u > 0 \\ &D_v f_u + D_u g_v > 0 \\ &(D_v f_u - D_u g_v)^2 + 4 D_u D_v f_v g_u > 0. \end{aligned} \tag{45}$$

Basically, the first two conditions in (45) correspond to the requirement that, in the absence of diffusion (cells are unconnected) the isolated cells are stable[10] ($\mathrm{Re}\lambda(0) < 0$). The last two conditions in (45) ensure the instability of the CNN when diffusion is present. Analyzing the above equations, one easily finds that, assuming $D_u, D_v > 0$, at least one of the coefficients in the first equation should be negative so that f_u and g_v must have opposite signs (in our case, $g_v < 0$). From the third equation, it follows that $f_u > 0$ and $D_v > D_u$. Thus, to have the second equation satisfied, we must have $f_v g_u < 0$. Hence, f_v and g_u must have opposite signs as well.

The domain in the parameter space for which the conditions for Turing instability are fullfilled will be called the Turing space of the CNN. Let us finally summarize the conditions for Turing pattern development in terms of the dispersion relation.

- A band of unstable modes exists, and the homogeneous spatial mode is stable: (45).
- There exists at least one spatial eigenvalue inside the band of unstable modes (corresponding to the imposed boundary conditions).
- The initial conditions should be such that at least one of the unstable modes could develop.
- The nonlinearity should be such that the growing pattern could evolve into a stable equilibrium.

Using straightforward calculations, one finds that the peak of the dispersion curve (Fig. 3); i.e., the value k^2 for which the derivative is zero, is located at the value

$$k_p^2 = \left[(g_v - f_u) + \frac{(D_u + D_v)}{\sqrt{D_u D_v}}\sqrt{-f_v g_u}\right]\frac{\gamma}{D_v - D_u} \tag{46}$$

where k_p^2 is real if $f_v g_u < 0$ and $D_v > D_u > 0$ and is positive if

$$(g_v - f_u)\sqrt{D_u D_v} + (D_u + D_v)\sqrt{-f_v g_u} > 0. \tag{47}$$

A band of unstable modes will exist for *real* intersection with the horizontal axis (real k_1^2 and k_2^2). Calculating the roots of $\mathrm{Re}\lambda(k^2) = 0$ and requiring them to be both real, we obtain the condition

$$-(f_u D_v - g_v D_u) + \sqrt{-f_v g_u}(D_u + D_v) > 0. \tag{48}$$

The limits of the band of unstable modes are the values k_1^2 and k_2^2

$$k_{1,2}^2 = \frac{\gamma}{2 D_u D_v}\Big[(D_v f_u + D_u g_v) \pm \sqrt{(D_v f_u - D_u g_v)^2 + 4 D_u D_v f_v g_u}\Big]. \tag{49}$$

Critical Values: When the two limits of the band of unstable modes concide, the dispersion curve is tangent to the k^2 axis (Fig. 4), and the linear system is at the limit of stability. This critical value k_c^2 of k^2 is given by

$$k_c^2 = \frac{\gamma(D_{vc} f_u + D_u g_v)}{2 D_u D_{vc}} = \gamma\sqrt{\frac{f_u g_v - f_v g_u}{D_u D_{vc}}} \tag{50}$$

where D_{vc} is the critical value of the diffusion coefficient D_v, obtained by setting to zero the square root in (49)

$$D_{vc} = \frac{(\sqrt{-f_v g_u} + \sqrt{f_u g_v - f_v g_u})^2}{f_u^2} D_u. \tag{51}$$

Let us make several observations concerning the influence of the dispersion coefficients on the behavior of the CNN. First, as it was already shown, the necessary Turing conditions cannot be satisfied with $D_u = D_v$. From the above formulae, we observe that, for $D_u \neq 0$ and $D_v \to \infty$, the band of unstable modes becomes $\{0, \frac{\gamma f_u}{2 D_u}\}$. In this case, the upper limit

[10] This is equivalent to the stability of the *constant* spatial mode for the whole CNN; namely, when $k_{mn}^2 = 0$ in (23) and (24).

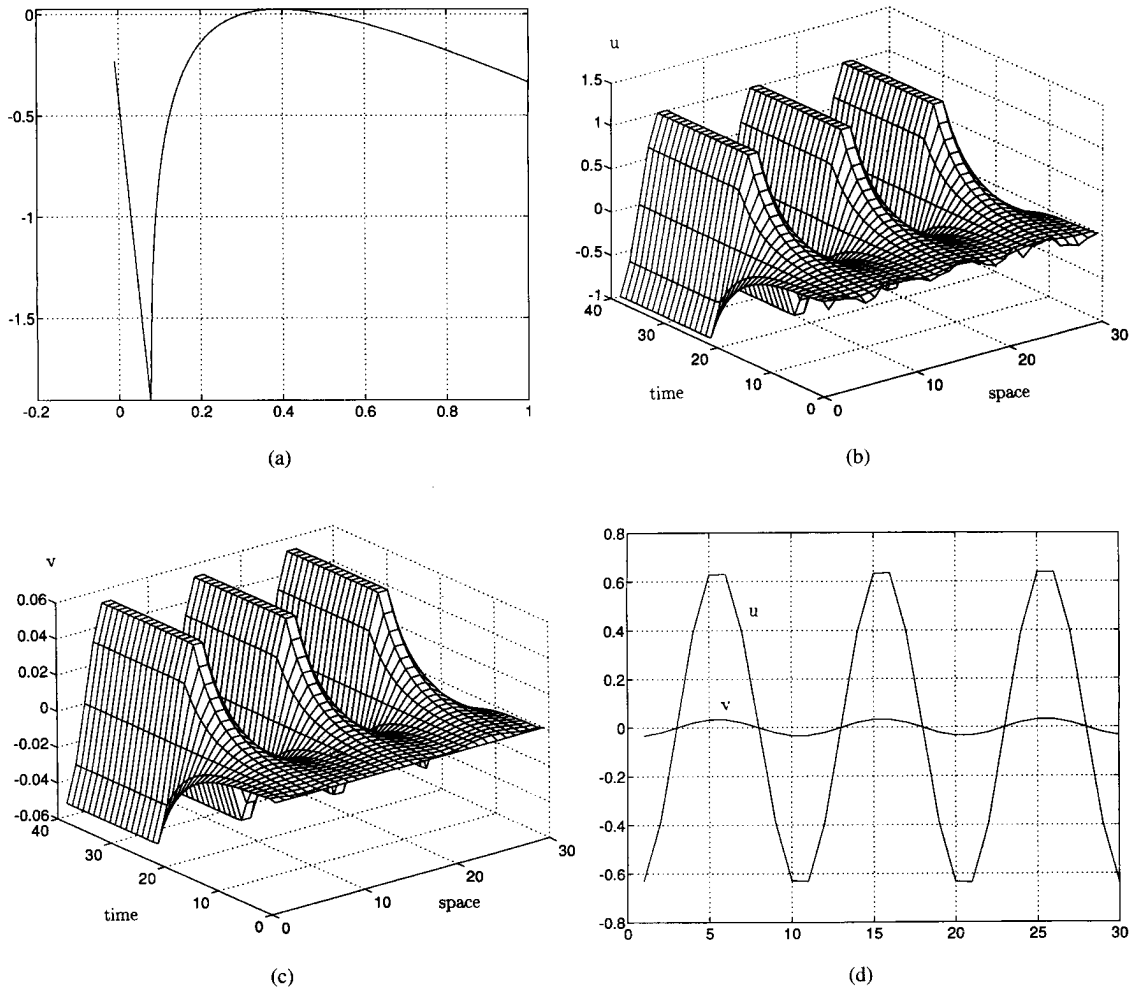

Fig. 5. (a) Dispersion curve for $\gamma = 8.5$, $D_v = 38$. Time evolution of the (b) u-voltage and (c) v-voltage for random initial conditions for u (max 0.1 amplitude) and zero initial conditions for v. Snapshots (d) at $t = 20$ and (e) at $t = 40$ from the evolutions of u and v. (f) and (g) Time evolution for initial conditions that do not contain the unstable spatial mode.

TABLE I

m n	0	1	2	3	4	5
0	0.00000	0.26795	1.00000	2.00000	3.00000	3.73205
1	0.38197	0.64992	1.38197	2.38197	3.38197	4.11402
2	1.38197	1.64992	2.38197	3.38197	4.38197	5.11402
3	2.61803	2.88598	3.61803	4.61803	5.61803	6.35008
4	3.61803	3.88598	4.61803	5.61803	6.61803	7.35008

of the band determines the lowest spatial eigenvalue that can belong to this band. Finally, for $D_u = 0$ ($R_u = \infty$); i.e., for the case of one-grid coupling, one can easily show, using (16) or (26) that the lower limit of the band of unstable modes is $k_1^2 = \frac{\gamma(f_u g_v - f_v g_u)}{D_v f_u}$ while the upper limit is infinite.

B. Role of Dispersion Curve and Initial Conditions in Pattern Formation

In this subsection, we will give examples for 1-D arrays illustrating how the periodic patterns appear. We will discuss the case of arrays having one and then several spatial unstable modes.

First Case—Only One Spatial Mode Unstable: The following example refers to a 1-D array of length $N = 30$ with zero-flux boundary conditions in the case when the band of unstable modes contains only one spatial eigenvalue. The eigenvalues for this case are shown in Table I.

Choosing $\gamma = 8.5$, $D_u = 1$, $D_v = 38$, and using cells with the parameters, $m_0 = 0.1$, $m_1 = m_2 = -1$, $\nu = 2$, $\epsilon = 0$, $E = 1$, $C_u = -0.2$, $C_v = 2$ (the elements of the Jacobian matrix are: $f_u = 0.1$, $f_v = -1$, $g_u = 0.1$, $g_v = -0.2$) we obtain the dispersion curve shown in Fig. 5(a) whose band of unstable modes, ranging from $k_1^2 = 0.30260$ to $k_2^2 = 0.50267$ contains only the 6th mode; i.e., the value $k_6^2 = 0.3819$. The dispersion curve has a peak of 0.02327 at $k_p^2 = 0.39069$. Using

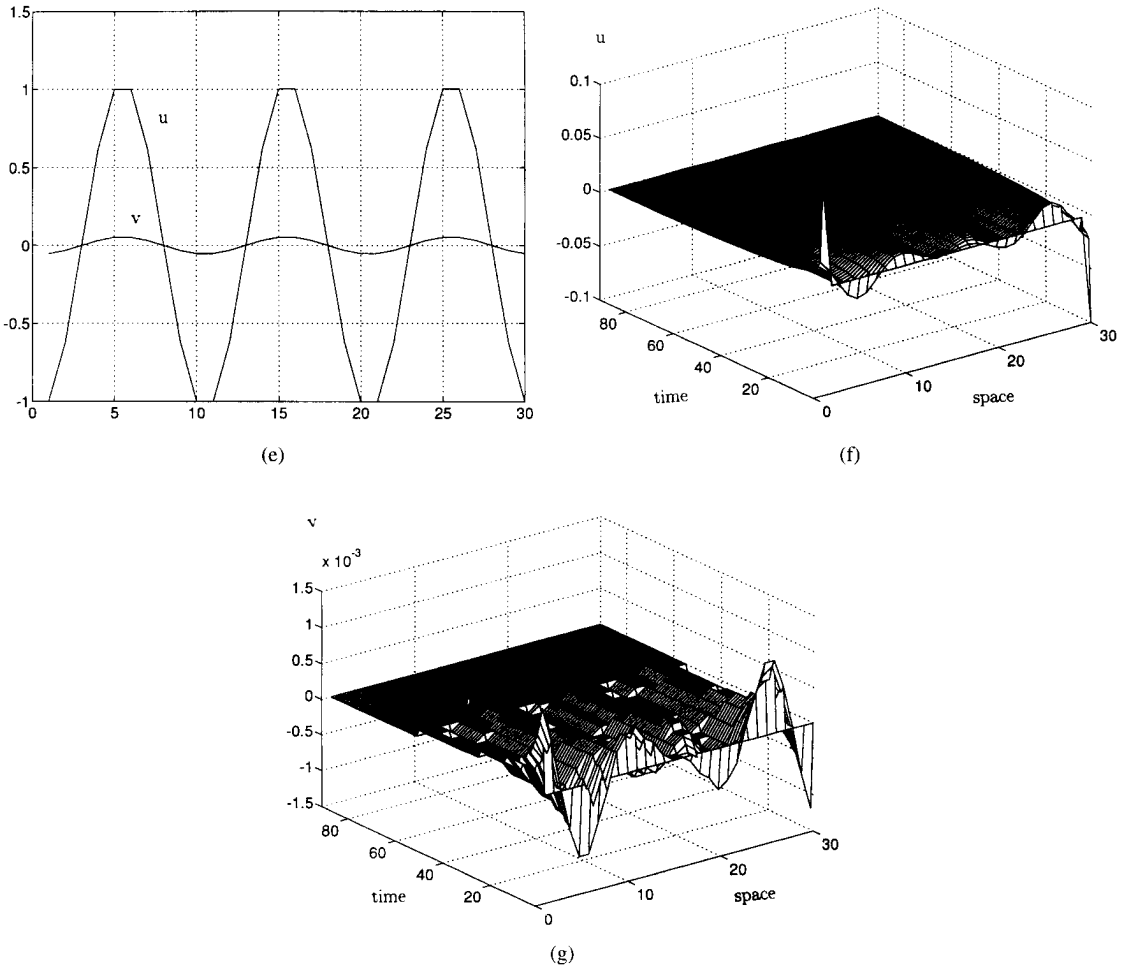

Fig. 5. *(Continued.)*

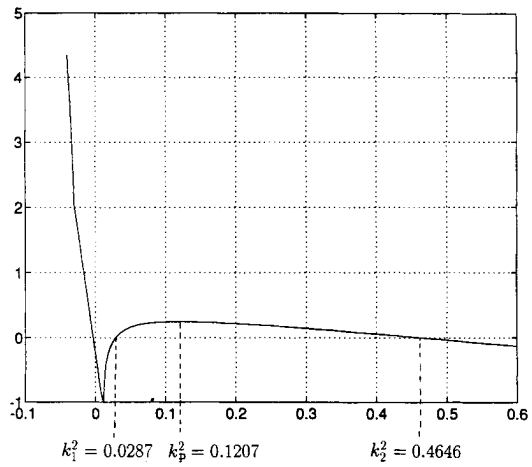

Fig. 6. Dispersion curve for $M = 30$, $\gamma = 5$, $f_u = 0.1$, $f_v = -1$, $g_u = 0.1$, $g_v = -2$, $D_u = 1$, and $D_v = 150$.

random initial conditions with maximum 0.1 amplitude, the time evolutions of the u- and v-voltages shown in Fig. 5(b) and (c) have been obtained. We show in Fig. 5(d) snapshots taken at time $t = 20$, before any cell reached the nonlinear region and in Fig. 5(e) at $t = 40$, when the pattern was already stabilized and some cells are in the nonlinear region (Fig. 5(d) and (e) are "sections" from Fig. 5(b) and (c) at two different time moments). In this case, the *only* spatial mode that can develop in the linear part of the transient is that corresponding to $m = 6$. The main points are that *the periodicity of the evolved pattern is determined by the (only) spatial unstable eigenmode* and *the nonlinearity did not change the periodic aspect of the pattern inherited from the linear part of the transient*; i.e., the pattern continues to be *periodic* with the same spatial period as it can be seen from Fig. 5(b) and (c) and also comparing Fig. 5(d) and (e). We remark that, by choosing appropriate parameters for the CNN, it is possible to select only one spatial mode. However, if the dimensions of the array are big, due to the fact that the adjacent spatial eigenvalues are very close to each other, their selection will be difficult because, on one hand, very careful tuning of the parameters is necessary and, on the other hand, the real part of the (only positive real part) selected temporal eigenvalue will be very small and thus, the transient will be very long. Moreover, if the initial conditions do not contain the above spatial mode, there will be no pattern assuming there is no noise, as shown for example in Fig. 5(f) and (g) for zero initial conditions except for the first and the last cell u-voltages, which are equal to $+0.1$ and -0.1, respectively, (in this case the 6th mode, which is a symmetric one, is not contained in the initial conditions).

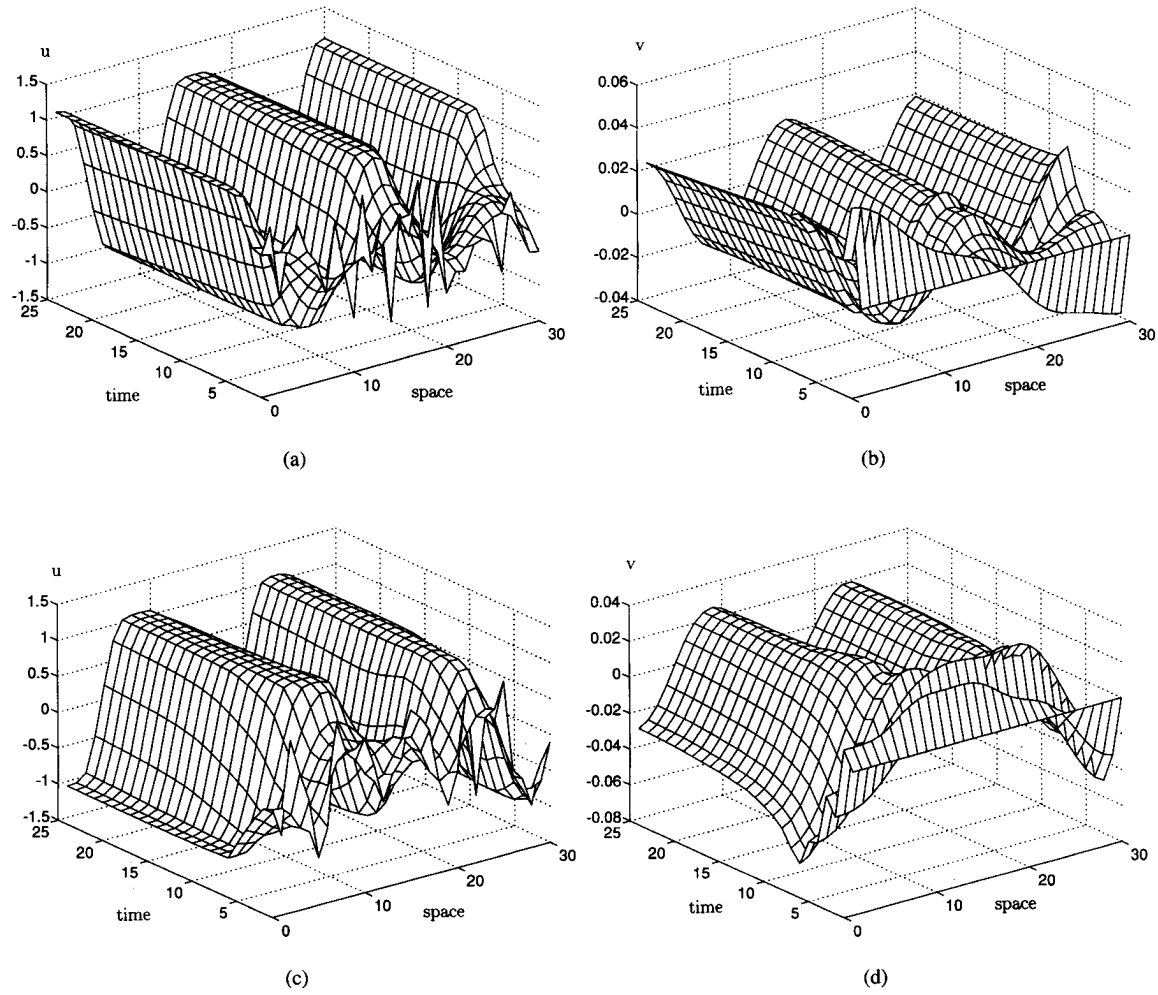

Fig. 7. Time evolutions for ,respectively, the (a) u-voltage and (b) v-voltage in a 1-D CNN with $M = 30$ subject to random initial conditions for the u-voltages and zero for the v-voltages; (c), (d) Same as above but with a different realization of the random initial conditions.

Second Case—Several Spatial Modes Unstable; No "Defects": Let us examine Fig. 3 for the 1-D case too. If, for instance, there are two eigenvalues k_a^2 and k_b^2 inside the band of unstable modes, at least two kinds of patterns could evolve: those corresponding to $\cos\frac{(2i+1)a\pi}{2M}$ and $\cos\frac{(2i+1)b\pi}{2M}$ (for zero-flux boundary conditions). Intuitively, the former is more likely to appear as it corresponds to a temporal eigenvalue with a greater real part. Indeed, this happens for random initial conditions when *the weights of the spatial modes are almost equal* so that the most favored mode wins. However, some appropriate choice of initial conditions could favor the appearance of the pattern corresponding to k_b^2 or even other patterns due to the influence of the nonlinearity. The following examples will be enlightening.

Consider again a 1-D CNN with $M = 30$. We choose the same parameters for the reduced Chua's circuit as above and the diffusion coefficients $D_u = 1$, $D_v = 40$. In this case, $\gamma = 5$ and the elements of the Jacobian matrix are: $f_u = 0.1$, $f_v = -1$, $g_u = 0.1$, $g_v = -0.2$. The corresponding dispersion curve is shown in Fig. 6. It has a peak of 0.25014 at $k_p^2 = 0.1207$, the limits of the band of unstable modes are $k_1^2 = 0.02870$ and $k_2^2 = 0.46464$, and the critical values are $D_{vc} = 35.88854$ and $k_c^2 = 2.36068$. There are five spatial eigenvalues inside the band of unstable modes; i.e., those corresponding to $m = 2$ to $m = 6$ and printed in boldface in Table I. We show in Fig. 7(a) and (b) the time evolution of $u_i(t)$ and $v_i(t)$ for $t \in [0, 25]$ and $i = 1 \cdots 30$ (the cells have been labeled from 1 to 30) for random initial conditions of maximum 0.5 amplitude for the u-voltages and zero for the v-voltages. We observe that the final pattern corresponds to $m = 4$, the value for which the real part of the associated temporal eigenvalue is the largest. Thus, even though the initial conditions were random, the final pattern is a distorted replica of the *most favored* spatial eigenfunction since all spatial modes have been excited with the same weight. Different realizations of the random conditions may produce the same pattern, or one having the opposite-phase, as happened in the case shown through the time evolutions in Fig. 7(c) and (d).

Next, we use deterministic initial conditions aiming to control the pattern evolution. This time the initial conditions will contain only one or two spatial modes with specified amplitudes and wavelengths. The time evolutions represented

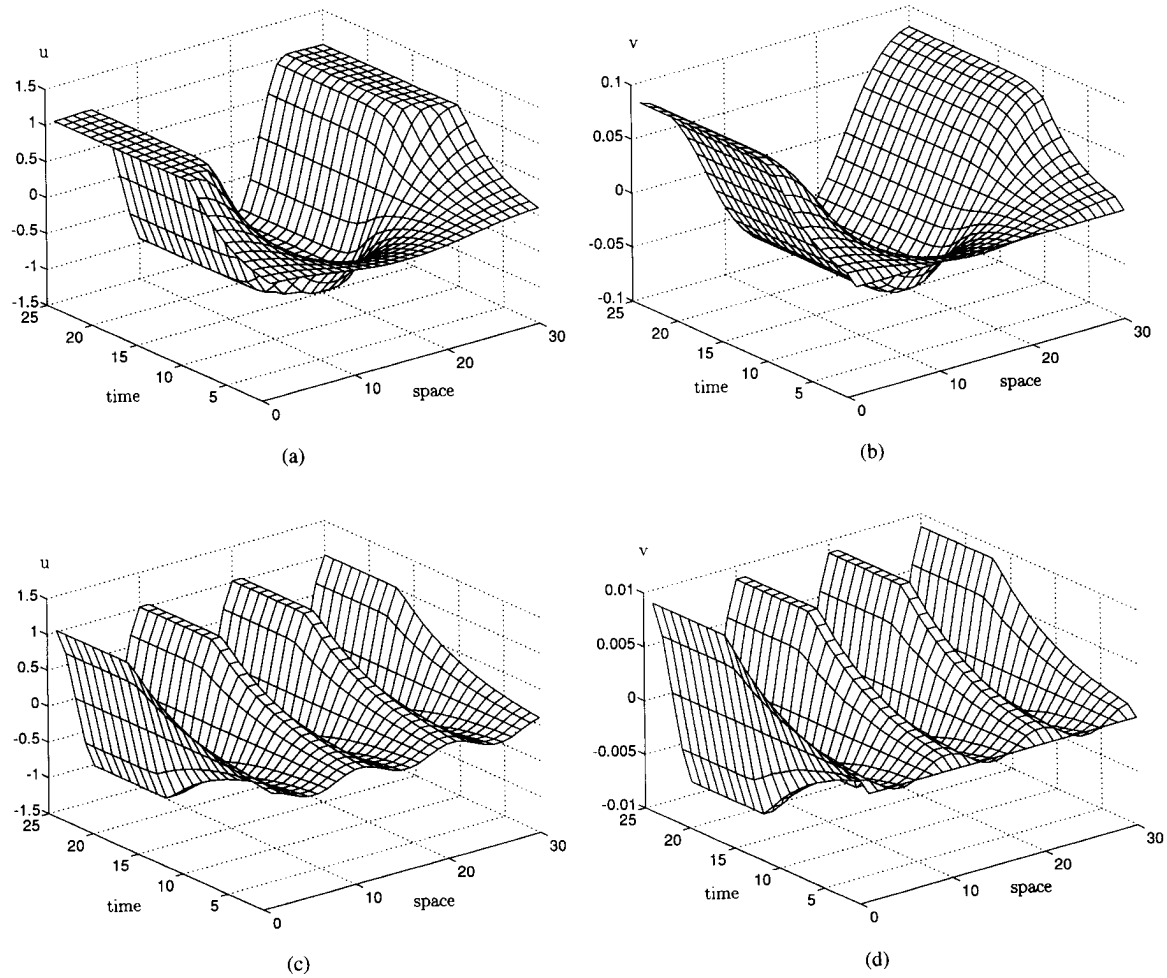

Fig. 8. Time evolutions of u- and v-variables for initial conditions for the u-voltages (and zero initial conditions for the v-voltages), chosen to excite the 2nd spatial mode (a) and (b) and the 6th spatial mode (c) and (d).

in Fig. 8(a) and (b) were obtained with the following initial conditions:

$$u_i(0) = 0.1 \cos \frac{(2i+1)m\pi}{2 \cdot 30}, \quad v_i(0) = 0, m = 2.$$

Thus, even though the real part of the temporal eigenvalue associated to the $m = 2$ mode is smaller, due to the fact that the weights of *all* spatial eigenvectors except for $m = 2$ are zero, the imposed pattern could be obtained. Using a similar procedure to excite only the 6-th spatial mode; i.e., using $m = 6$ in the above initial condition, we obtained the evolutions shown in Fig. 8(c) and (d).

The following results have been obtained using u-initial conditions containing both spatial modes $m = 2$ and $m = 6$ with various amplitudes ($v_i(0) = 0$ as before)

$$u_i(0) = A \cos \frac{(2i+1)2\pi}{2 \cdot 30} + B \cos \frac{(2i+1)6\pi}{2 \cdot 30}.$$

The time evolutions shown in Fig. 9(a) and (b) have been obtained for $A = B = 0.1$; observe that the most favored spatial eigenfunction is that corresponding to $m = 2$. The patterns in Fig. 9(c) and (d) were obtained for $A = 0.1$ and $B = 0.2$; observe that still the pattern corresponding to $m = 2$ has been selected even though its initial weight was smaller. However, in this case, the tendency to develop the 6-th spatial mode is apparent. In both cases, the final pattern has the same shape.

Using $A = 0.1$ and $B = 0.4$, we observe from the time evolution shown in Fig. 9(e) and (f) that already the 6th spatial mode has been selected. Finally, using u-initial conditions corresponding to $m = 8$ (i.e., a spatial mode placed outside the band of unstable modes) and zero for the v-voltages as before, we obtained the time evolutions shown in Fig. 10(a) and (b); i.e., all cells evolved to the (*unstable*) homogeneous equilibrium point (U_0, V_0).

Remark: The above behavior assumes an ideal noise-free CNN. In a physical CNN, the inherent noise will, however, determine the emergence of a pattern, the most probable evolution being one of those already shown in Fig. 7 since in this case all modes will be excited and the imposed initial conditions will not influence the CNN.

Third Case—Many Spatial Modes Unstable; "Defects": The example that follows was obtained for a similar 30 cells 1-D CNN, the only parameters that were changed being $\gamma = 15$ and $D_v = 250$. In this case, the dispersion curve,

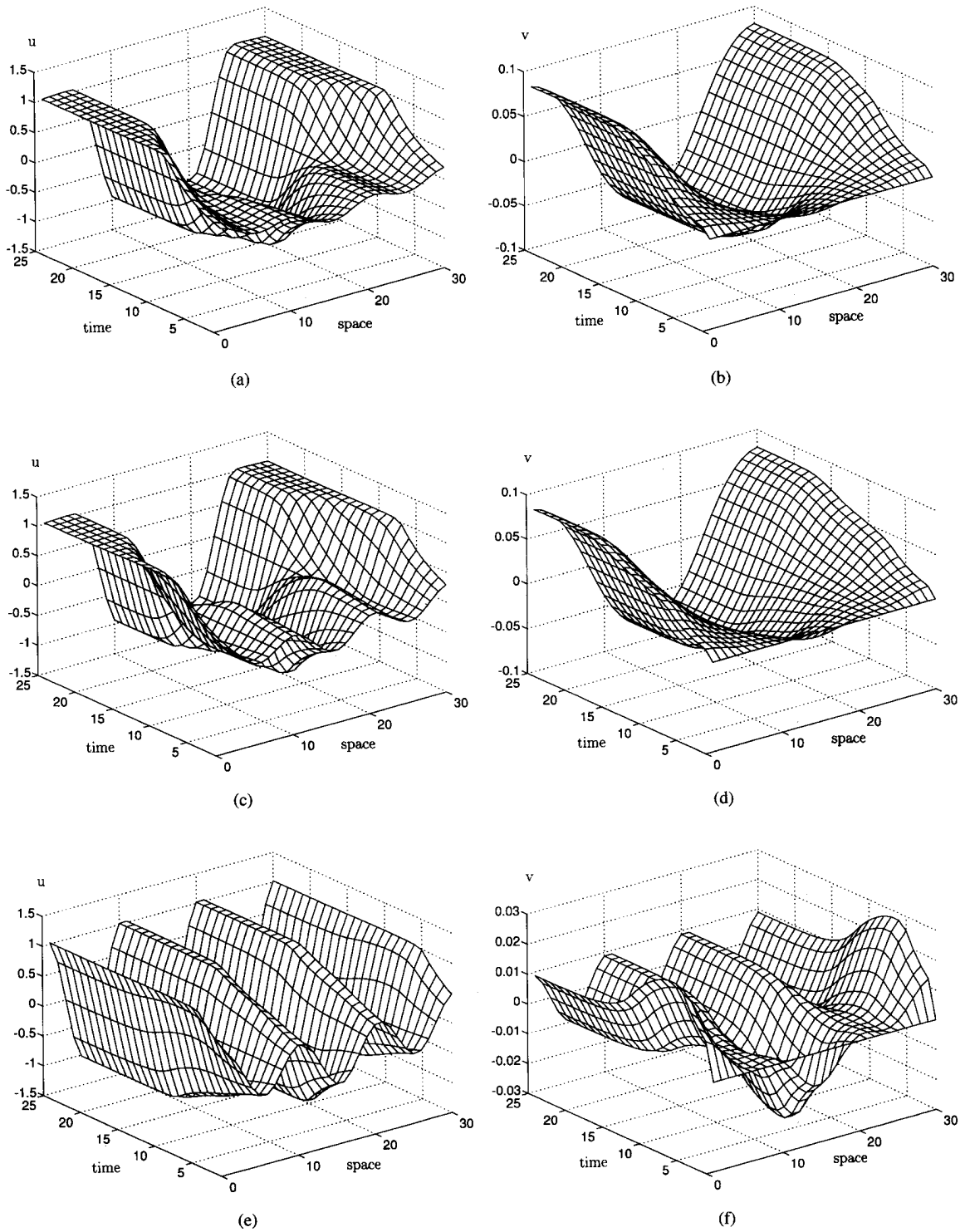

Fig. 9. Time evolutions of u- and v-variables for u-initial conditions containing two spatial components and zero initial conditions for the v-voltages (see text).

represented in Fig. 11(a), contains ten spatial eigenvalues (for $m = 3$, $k_3^2 = 0.0978$ to $m = 12$, $k_{12}^2 = 1.3819$). Using random initial conditions of unity amplitude for the u-variable and zero initial conditions for the v-variables, the evolutions shown in Fig. 11(b) and (c) have been obtained, and the final stable patterns are represented in Fig. 11(d). We remark the fact that the final pattern, even though approximately periodic, contains "defects" that have been produced by the conjugate effects of the high amplitude of the initial conditions: they affect the transient and the large band of unstable modes, thereby allowing a competition between many modes.

Similar examples can be produced for 2-D arrays as well. However, in general, it is virtually impossible to predict the final pattern. The nonlinearities can play a decisive role, and patterns having no resemblance to those predicted by linear theory considerations may emerge.

TABLE II

k_0^2 =0.0000	k_1^2 =0.0109	k_2^2 =**0.0437**	k_3^2 =**0.0978**	k_4^2 =**0.1729**	k_5^2 =**0.2679**
k_6^2 =**0.3819**	k_7^2 =05137	k_8^2 =0.6617	k_9^2 =0.8244	$k_1 0^2$ =1.0000	$k_1 1^2$ =1.1865
$k_1 2^2$ =1.3819	$k_1 3^2$ =1.5841	$k_1 4^2$ =1.7909	$k_1 5^2$ =2.0000	$k_1 6^2$ =2.2090	$k_1 7^2$ =2.4158
$k_1 8^2$ =2.6180	$k_1 9^2$ =2.8134	$k_2 0^2$ =3.0000	$k_2 1^2$ =3.1755	$k_2 2^2$ =3.3382	$k_2 3^2$ =3.4862
$k_2 4^2$ =3.6180	$k_2 5^2$ =3.7320	$k_2 6^2$ =3.8270	$k_2 7^2$ =3.9021	$k_2 8^2$ =3.9563	$k_2 9^2$ =3.9890

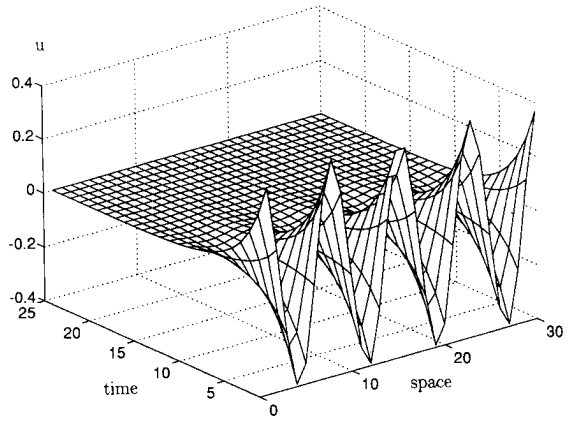

(a)

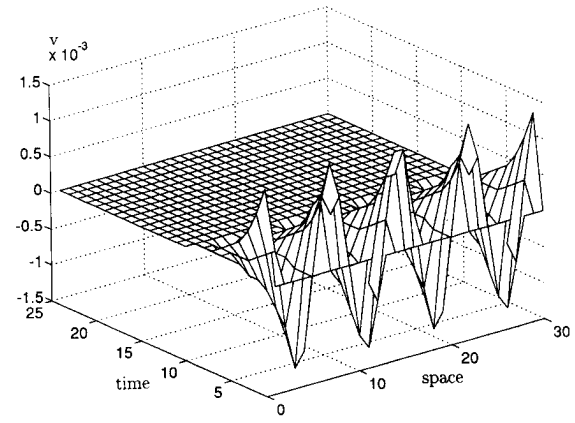

(b)

Fig. 10. Time evolutions of (a) u-variable and (b) v-variable for u-initial conditions containing only the 8th spatial mode placed outside the band of unstable modes and zero v-initial conditions.

APPENDIX I
SPATIAL EIGENVALUES k_{mn}^2 FOR $M = 5$, $N = 6$ AND ZERO-FLUX BOUNDARY CONDITIONS

The eigenvalues have been calculated using the relation

$$k_{mn}^2 = 4\left(\sin^2\frac{m\pi}{2M} + \sin^2\frac{n\pi}{2N}\right)$$

(see (37)) with $M = 5$, $N = 6$, $m = 0, \cdots, 4$, and $n = 0, \cdots, 5$. (See Table II).

APPENDIX II
THE DISCRETE EXPONENTIAL FUNCTIONS AS EIGENFUNCTIONS OF THE DISCRETE LAPLACIAN

In general, λ_a is called an *eigenvalue* of the linear operator $\mathbf{L}$ associated with the *eigenfunction* ϕ_a if $\mathbf{L}\phi_a = \lambda_a\phi_a$. In the following, we show that functions of the form e^{ai+b} where i is the space index, a may be complex, and b is real, are eigenfunctions of the 1-D discrete Laplacian operator $\mathbf{L} = \nabla^2$ and $\lambda_a = 4\sinh^2\frac{a}{2}$ are the corresponding eigenvalues.[11] Indeed,

$$\begin{aligned}\nabla^2 e^{ai+b} &= e^{a(i+1)+b} + e^{a(i-1)+b} - 2e^{ai+b}\\ &= (e^a + e^{-a} - 2)e^{ai+b} = 4\sinh^2\frac{a}{2}\cdot e^{ai+b}.\end{aligned}$$

In particular, for $a = j\alpha$, where $j = \sqrt{-1}$ we have $\nabla^2 e^{j\alpha i+b} = 4\sinh^2\frac{j\alpha}{2}\cdot e^{j\alpha i+b} = -4\sin^2\frac{\alpha}{2}\cdot e^{j\alpha i+b}$ and, taking the real parts, $\nabla^2\cos(\alpha i+b) = -4\sin^2\frac{\alpha}{2}\cos(\alpha i+b)$. In these cases, appropriate for the analysis we made in this paper, if we denote $k_\alpha = 2\sin\frac{\alpha}{2}$, the eigenvalues are $\lambda_\alpha = -k_\alpha^2$. Observe that the eigenvalues do not depend on the initial phase b of the exponential or cosine functions.

APPENDIX III
CONTINUOUS-SPACE CASE

In the following, we briefly discuss the continuous-space version of the two-grid coupled CNNs. In this case, the grids will be replaced by sheets of homogeneous conducting materials.[12] The aim is twofold: on the one hand, the equations we are going to derive are identical to those describing continuous pattern phenomena in physics, chemistry, ecology, and biology. On the other hand, the previously derived equations can be viewed as resulting from a discretization of the distributed or continuous-space problem; in this situation, the discrete equations *approximate* the continuous-space ones. Following a procedure similar to the derivation of the telegraphers' equations; i.e., writing KCL for the infinitesimal nodes (x, y) similar to (i, j) of Fig. 1 and using the well-known fact that the conductance is proportional to the transversal dimension and inversely proportional to the longitudinal dimension, we have

$$\begin{cases} C_u\Delta x\Delta y\frac{\partial u_{x,y}(t)}{\partial t}\\ = -i_1(u_{xy}, v_{xy})\Delta x\Delta y + G_u\frac{\Delta y}{\Delta x}(\Delta_1 u_{xy} - \Delta_2 u_{xy})\\ \quad + G_u\frac{\Delta x}{\Delta y}(\Delta_3 u_{xy} - \Delta_4 u_{xy})\\ C_v\Delta x\Delta y\frac{\partial v_{x,y}(t)}{\partial t}\\ = -i_2(u_{xy}, v_{xy})\Delta x\Delta y + G_v\frac{\Delta y}{\Delta x}(\Delta_1 v_{xy} - \Delta_2 v_{xy})\\ \quad + G_v\frac{\Delta x}{\Delta y}(\Delta_3 v_{xy} - \Delta_4 v_{xy}).\end{cases} \tag{52}$$

Dividing by $\Delta x\Delta y$ and passing to the limit, we obtain

$$\begin{cases}\frac{\partial u(x,y,t)}{\partial t} = -\frac{1}{C_u}i_1(u(x,y,t), v(x,y,t)) + \frac{G_u}{C_u}\nabla^2 u(x,y,t)\\ \frac{\partial v(x,y,t)}{\partial t} = -\frac{1}{C_v}i_2(u(x,y,t), v(x,y,t)) + \frac{G_v}{C_v}\nabla^2 v(x,y,t)\end{cases} \tag{53}$$

where C_u, C_v, G_u, and G_v are the distributed (per unit area) "surface" capacitance, and conductance, and ∇^2 is the continuous 2-D Laplacian.

[11] The 2-D case follows as a generalization using (35) and (36).

[12] The physical realization of such "distributed" CNNs would have to face the problem of the ground plane that should exist between the two external plates.

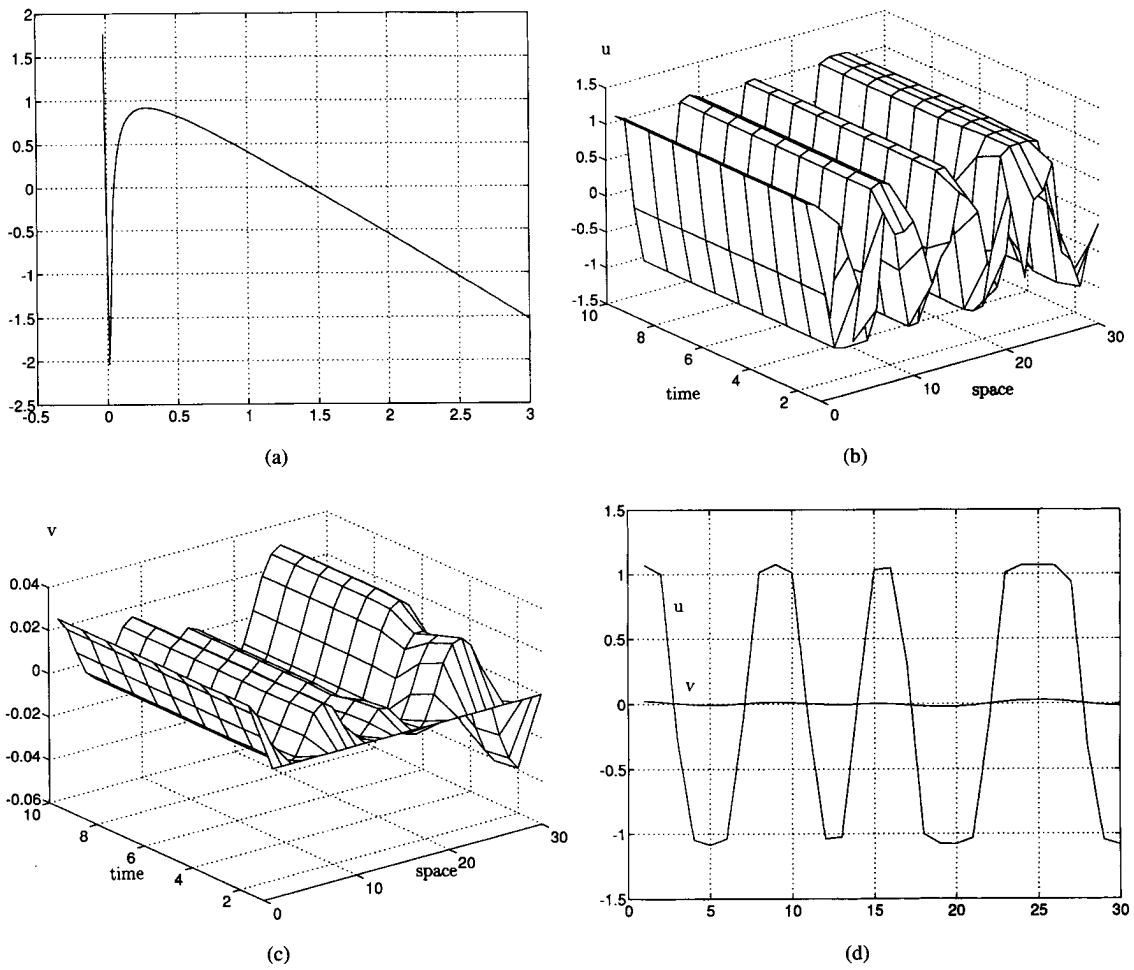

Fig. 11. (a) Dispersion curve for $\gamma = 15$ and $D_v = 250$. Time evolutions of u- (b) and v-variables (c) for random initial conditions for the u-voltages (and zero initial conditions for the v-voltages); (d) Final patterns with "defects."

Straightforward normalization gives the equations:

$$\begin{cases} \frac{\partial u(x,y,t)}{\partial t} = \gamma f(u(x,y,t), v(x,y,t)) + D_u \nabla^2 u(x,y,t) \\ \frac{\partial v(x,y,t)}{\partial t} = \gamma g(u(x,y,t), v(x,y,t)) + D_v \nabla^2 v(x,y,t) \end{cases} \tag{54}$$

which are the reaction–diffusion equations describing Turing-pattern phenomena in many areas of science; e.g., biology. Of course, to solve the above equations, initial conditions of the form $u(x,y,0)$ and $v(x,y,0)$ as well as boundary conditions which, in particular, may be zero, zero-flux, etc., must be given.

VIII. Concluding Remarks

Even though the Turing pattern formation is intrinsically a nonlinear process, the linear theory developed above has sufficient power to predict not only the conditions for Turing instability but also certain qualitative features of the final pattern. The problem of Turing pattern generation in the two-grid coupled CNN was investigated by decoupling a large system of linear differential equations into pairs of linear differential equations. No matter how large the array is, this spatio-temporal decoupling technique reduces the analysis of pattern formation to the analysis of an uncoupled system of two first-order linear differential equations directly related to the spatial eigenvectors. The influence of the initial and boundary conditions and their relation to the spatial eigenvectors and eigenvalues are derived. Computer simulation results are presented in Part III of this paper.

References

[1] L. Goraş, L. O. Chua, and D. M. W. Leenaerts, "Turing patterns in CNNs—Part I: Once over lightly," *IEEE Trans. Circuits Syst. I*, vol. 42, no. 10, pp. 602–611, this issue.
[2] R. Madan, *Chua's Circuit: A Paradigm for Chaos.* Singapore: World Scientific, 1993.
[3] J. D. Murray, *Mathematical Biology.* Berlin: Springer-Verlag, 1989.
[4] A. Pérez-Muñuzuri, V. Pérez-Muñuzuri, M. Gómez-Gesteira, and L. O. Chua, "Spatio-temporal structures in discretely-coupled arrays of nonlinear circuits: A review," *Int. J. Bifurc. and Chaos*, vol. 5, no. 1, pp. 17–50, Feb. 1995.
[5] P. M. DeRusso, R. J. Roy, and C. M. Close, *State Variables for Engineers.* New York: Wiley, 1965.
[6] K. R. Rao and P. Yip, *Discrete Cosine Transform: Algorithms, Advantages and Applications.* Boston: Academic, 1990.
[7] A. Papoulis, *Signal Analysis.* New York: McGraw Hill, 1977.

Liviu Goraş (M'91), for a photograph and biography, see this issue, p. 611.

Leon O. Chua (S'60–M'62–SM'70–F'74), for a photograph and biography, see this issue, p. 558.